

# Poly(lactide)/cellulose nanocrystals: the *in situ* polymerization approach to improved nanocomposites

Stefano Gazzotti,<sup>a,b</sup> Hermes Farina,<sup>a,b</sup> Giordano Lesma,<sup>a,b</sup> Riccardo Rampazzo,<sup>a</sup> Luciano Piergiovanni,<sup>b,c</sup> Marco Aldo Ortenzi,<sup>a,b,\*</sup> Alessandra Silvani<sup>a,b</sup>

<sup>a</sup> Dipartimento di Chimica, Università degli Studi di Milano, via Golgi 19, Milano, 20133, Italy.

<sup>b</sup> CRC Materiali Polimerici "LaMPO", Dipartimento di Chimica, Università degli Studi di Milano, via Golgi 19, Milano, 20133, Italy.

<sup>c</sup> DeFENS, Department of Food, Environmental and Nutritional Sciences, Università degli Studi di Milano, via Celoria 2, Milano, 20133, Italy.  
\*E-mail: marco.ortenzi@unimi.it

**Keywords:** Poly(lactic Acid), Cellulose Nanocrystals, Nanocomposite, *In Situ* Synthesis, Thermal stability.

The *in situ* polymerization of L-lactide in the presence of various amounts of cellulose nanocrystals (CNC) is described. CNC was prepared efficiently by acidic hydrolysis of cotton linters. Molecular weight, morphology, thermal, mechanical and crystallization properties of the PLA-CNC nanocomposites were evaluated. From size-exclusion chromatography (SEC) analysis, the actual occurrence of chemical bond between CNC and PLA can be assessed. The effect of CNC has been evaluated through differential scanning calorimetry (DSC) analysis, which highlights the probable formation of  $\alpha'$  crystals in the obtained materials. More importantly, from thermogravimetric analysis (TGA) a marked improvement in thermal stability of nanocomposites has been demonstrated, with respect to standard PLA and to previously described PLA-CNC blends. Nanocomposites show also an improvement in rheological properties with respect to standard PLA. In particular, storage modulus greatly increases, indicating a reinforcing effect of CNC. The described *in situ* synthetic methodology allows an optimal compatibilization between the two entities (PLA and CNC), facing one of the major problems inherent to the preparation of nanocomposites. It leads furthermore to remarkably improved thermal and rheological properties of the obtained materials.

## Introduction

In recent years environmental awareness has been focused onto the replacing of traditional plastics based on petrochemical resources with alternative, more eco-friendly materials. Among them, poly(lactic acid), shortly PLA, is one of the most attractive to researchers and industry,<sup>1</sup> because of its good biodegradability and availability from renewable sources, such as starch and sugar beet.<sup>2</sup> The growing attention towards this thermoplastic polymer comes from both its outstanding properties, such as the good optical and elastic behavior and the excellent melt-processability, and, at the same time, from its cost competitiveness, also with respect to more traditional, not biodegradable polyesters such as PET.<sup>3,4</sup> For all these reasons, nowadays PLA has gained commercial significance and greatly increased its market, especially for what regards packaging and disposables applications.

However, PLA suffers from a lot of drawbacks that strongly limit possibilities for its wide application in many sectors. Indeed, it is endowed with low thermal and mechanical stability upon processing conditions, scarce flexibility and poor barrier properties. All these characteristics place it behind commonly used plastics, for instance for food packaging applications.<sup>5</sup>

Among possible alternatives to overcome some of these limitations, the preparation of nanocomposites has emerged as the most promising suitable solution.<sup>6</sup> In nanocomposites, the surface area/volume ratio of employed reinforcement additives is crucial to the enhancement of material properties. Indeed, as dimensions reach the nanometer level, interactions at phase interfaces become largely improved, bringing nanocomposites to exhibit properties not expected with larger scale particulate reinforcements. A lot of different additives can in principle be used as nanofillers. Among others, carbon nanotubes,<sup>7,8</sup> montmorillonite<sup>9,10</sup> and nanosilica<sup>11,12</sup> have been studied, with satisfactory achievements, in the design of PLA nanocomposites.

Aiming to produce fully organic bionanocomposites, cellulose nanocrystals (CNC) have recently emerged as a kind of biocompatible, biodegradable and renewable additive that could be dispersed into the PLA polymer matrix for the preparation of high performance blends. CNC are acquiring more and more interest in several

54 fields of application thanks to unique chemical and mechanical properties. They are rod-like particles with  
55 extremely high aspect ratio, high Young modulus, low density and high surface area. CNC can be extracted  
56 from almost every cellulose source, with different extraction methods properly described in literature.<sup>13, 14</sup>  
57 <sup>15</sup> Basically, they all rely onto the disruption of amorphous regions in cellulose fibers that are more susceptible  
58 of reaction (acid hydrolysis or oxidation reactions mainly), while preserving crystalline regions that can be  
59 isolated. Alongside the cited outstanding physical properties, the carbohydrate nature of these crystals  
60 ensures interesting chemical properties. The presence of a great quantity of free hydroxyl groups, primary  
61 and secondary, on CNC surface can be both a drawback and an advantage when blends with PLA are  
62 prepared. In fact, at a first glance, the high polarity of CNC clashes with the relatively apolar nature of PLA,  
63 resulting in dispersion problems that can seriously impact the properties of the obtained composite material.  
64 On the other side, however, the high quantity of reactive moieties on CNC opens to a lot of possible chemical  
65 derivatizations, that can be exploited in order to confer better compatibility with the polymer matrix.  
66 Various preparation methods have been developed to obtain biocomposites by blending PLA with different  
67 amounts of CNC.<sup>16, 17</sup> In some of these biocomposites, CNC have been preventively chemically modified in  
68 order to improve the interfacial adhesion with the polymer matrix.<sup>18, 19</sup> One effective method for chemical  
69 modification of CNC is to grow polymers directly off their surface, using the "grafting-from" approach.<sup>20</sup> By  
70 this way, short PLA oligomers have been successfully grafted from CNC using a ring-opening polymerization  
71 (ROP) protocol, affording PLA-bearing CNC, which were then blended with PLA.<sup>21, 22, 23</sup> Quite recently, a  
72 further enhancement of compatibilization of CNC with the PLA matrix was described by Dhar and co-workers,  
73 who employed a reactive extrusion process in order to graft PLA chains onto CNC through a radical reaction.<sup>24</sup>  
74 In PLA-CNC nanocomposites obtained via compounding, thermal degradation of both PLA and CNC during  
75 extrusion is an unsolved issue. Only small improvements in thermal stability of the obtained materials are  
76 reported in few cases, especially when reactive extrusion is carried out in the presence of chain extenders  
77 and radical initiators.<sup>25</sup>  
78 On the basis of our related experience on preparation of PLA nanocomposites containing nanosilica (NS)<sup>11</sup> or  
79 modified montmorillonite (MMT)<sup>9</sup>, we looked at PLA-CNC nanocomposites via the *in situ* polymerization of  
80 L-lactide in the presence of various amounts of CNC.  
81 It is well established that *in situ* polymerization in the presence of fillers provides distinct advantages when  
82 compared to other nanocomposite synthesis techniques, appearing more appropriate in providing excellent  
83 dispersion of the nanoparticles, which should have a greater impact on achievable properties. The *in situ*  
84 polymerization technique has been recently applied for the preparation of various PLA nanocomposites,  
85 incorporating for instance TiO<sub>2</sub><sup>26</sup> or MMT fillers.<sup>27</sup> Marked improvements in thermal properties and  
86 crystallinity of the resultant composites were obtained, compared to those of the standard polymers.  
87 To the best of our knowledge, no *in situ* polymerization strategies employing CNC have been described for  
88 the preparation of PLA nanocomposites. In this study, the *in situ* polymerization of L-lactide was performed  
89 with different loading ratios of CNC, prepared by acidic hydrolysis of cotton linters. The protocol exploits the  
90 alcoholic moieties of CNC as initiators in ring opening polymerization reaction of L-lactide. Molecular weight,  
91 morphology, thermal, mechanical and crystallization properties of the obtained nanocomposites were  
92 evaluated.

## 94 **Experimental**

### 96 **Synthesis of Cellulose Nanocrystals**

97 Cellulose nanocrystals were obtained by acidic hydrolysis, as described in literature.<sup>15</sup> Triturated cotton  
98 linters were slowly added to a preheated solution of 64 % w/w sulfuric acid. The ratio fiber : sulfuric acid was  
99 1 : 17.5 g/mL. The cotton hydrolysis was performed under vigorous stirring at 45 °C for 45 min. After this  
100 period, the solution was diluted with 10 times-volume deionized water in order to stop the acidic hydrolysis.  
101 The suspension was then centrifuged at least 5 times at 10000 rpm for 20 minutes each round. The  
102 precipitated solid was repeatedly rinsed and centrifuged with deionized water. In order to remove the acid  
103 excess, the centrifuged solution was put into a dialysis tubes immersed in deionized water for 3 days. The  
104 suspension was then sonicated repeatedly (0.7 cycles of 15 min at 70 % output) to create cellulose crystals  
105 of colloidal dimensions. In order to complex any stray ions, an ion-exchange resin was put into the dispersion  
106 for 24 hours at room temperature. After resin removal, the suspension was filtered under vacuum with a

107 Whatman glass microfiber filter to remove the largest cellulose-fiber agglomerates. Finally, the dispersion  
108 was lyophilized using a lab lyophilizer, obtaining a white-dried powder.

#### 109 **Synthesis of PLA**

110 PLA was synthesized from L-lactide in bulk according to the following procedure. L-lactide (25 g) and tin  
111 octanoate (0.3 % w/w on lactide), added as catalyst, were introduced in a 250 mL three necked round  
112 bottomed flask. Slow nitrogen flow was used to ensure the presence of inert atmosphere during  
113 polymerization reaction. Mechanical stirring was provided (40 rpm). Reaction was conducted in a closed oven  
114 at 180 °C for 2 hours. At the end of the reaction, the polymer was left cooling overnight under nitrogen  
115 atmosphere.

#### 116 **Synthesis of PLA-CNC nanocomposites**

117 Nanocomposites were synthesized by *in situ* polymerization, from L-lactide in bulk according to the following  
118 procedure. CNC in different quantities, from 0.125 grams – used to synthesize PLA0.5 – to 1.250 grams –  
119 used to synthesize PLA5 (see **Table 1**), were put in a three-necked round bottomed flask and dispersed in 50  
120 mL of acetone under vigorous stirring and ultrasound treatment. This procedure ensures the disaggregation  
121 of the lyophilized CNC fluffy mass into single crystals.

122 25 g of L-lactide were then added and left under stirring until complete dissolution. Acetone was then  
123 evaporated using nitrogen flux. The reaction mixture was then heated to 70 °C under vacuum in a closed  
124 oven for 2 hours in order to remove any residual moisture. After this drying step, reaction was performed  
125 following the procedure described for the synthesis of PLA. Five nanocomposites samples (PLA0.5, PLA2,  
126 PLA2.5, PLA3, PLA5) were prepared varying the percentage of employed CNC (see Table 1).

Sample	Cellulose Nanocrystals	
	(%wt)	(g)
PLA	0	0
PLA0.5	0.5	0.125
PLA2	2	0.500
PLA2.5	2.5	0.625
PLA3	3	0.750
PLA5	5	1.250

129 **Table 1:** Samples synthesized and CNC relative and absolute quantities.

#### 130 **Characterization**

131 **Size Exclusion Chromatography (SEC).** The effect of CNC on the molecular weight of obtained  
132 nanocomposites was evaluated using a SEC system having Waters 1515 Isocratic HPLC pump and a four  
133 Waters Styragel columns' set (HR3-HR4-HR5-HR2) with an UV detector Waters 2487 Dual  $\lambda$  Absorbance  
134 Detector set at 230 nm using a flow rate of 1 mL/min and 60  $\mu$ L as injection volume. Samples were prepared  
135 dissolving 50 mg of polymer in 1 mL of anhydrous  $\text{CH}_2\text{Cl}_2$  and filtering the solution on 0.45  $\mu$ m filters. Given  
136 the relatively high loading, a check was performed using lower concentration of polymer (5mg/mL), in order  
137 to verify that no column overloading could be observed. Anyway higher loadings were preferred as UV signal  
138 of PLA is relatively weak.

139 Molecular weight data are expressed in polystyrene (PS) equivalents. The calibration was built using  
140 monodispersed PS standards having the following nominal peak molecular weight  
141 (Mp) and molecular weight distribution (D): Mp=1,600,000 Da (D $\leq$ 1.13), Mp=1,150,000 Da (D $\leq$ 1.09),  
142 Mp=900,000 Da (D $\leq$ 1.06), Mp=400,000 Da (D $\leq$ 1.06), Mp=200,000 Da (D $\leq$ 1.05), Mp= 90,000 Da (D $\leq$ 1.04),  
143 Mp=50,400 Da (D=1.03), Mp=30,000 Da (D=1.06), Mp=17,800 Da (D=1.03), Mp=9,730 Da (D=1.03), Mp=5,460  
144 Da (D=1.03), Mp=2,032 Da (D=1.06), Mp=1,241 Da (D=1.07), Mp=906 Da (D=1.12), Mp=478 Da (D=1.22); Ethyl  
145 benzene (molecular weight=106 g/mol). For all analyses, 1,2-dichlorobenzene was used as internal reference.

160  
161 **Differential Scanning Calorimetry (DSC).** DSC analyses were conducted using a Mettler Toledo DSC1, on  
162 samples weighting from 5 to 10 mg each. Melting and crystallization temperatures were measured using the  
163 following temperature cycles:  
164 1. Heating from 25 °C to 200 °C at 10 °C/min;  
165 2. 5 min isotherm at 200 °C;  
166 3. Cooling from 200 °C to 25 °C at 10 °C/min;  
167 4. 2 min isotherm at 25 °C;  
168 5. Heating from 25 °C to 70 °C at 10 °C/min;  
169 6. Heating from 70 °C to 200 °C at 5 °C/min.  
170 The first two cycles were run to eliminate residual internal stresses deriving from the synthesis. Glass  
171 transition temperature ( $T_g$ ), cold crystallization temperature ( $T_c$ ) and melting temperature ( $T_m$ ) were  
172 determined. The lower heating rate in the last cycle (i.e. cycle number 6) was used in order to better separate  
173 the cold crystallization and melting peaks.  
174  
175 **Thermogravimetric Analysis (TGA).** TGA were performed using a TGA 4000 Perkin Elmer instrument; tests  
176 were conducted in air on samples weighting from 5 to 10 mg each, with a program that provides a single  
177 heating cycle from 30 °C to 800 °C at 10 °C/min.  
178  
179 **Rheological Curves.** Rheological analyses, conducted using frequency sweep experiments, were performed  
180 with a Physica MCR 300 rotational rheometer with a parallel plate geometry (diameter = 25 mm, distance  
181 between plates = 1 mm). Linear viscoelastic regimes of neat PLA and PLA nanocomposites were studied;  
182 strain was set equal to 5% and curves of complex viscosity as function of frequency were recorded, taking 30  
183 points ranging from 100 Hz to 0.1 Hz with a logarithmic progression, at 190 °C.  
184  
185 **Wide Angle X-Ray Scattering (WAXS).** Wide Angle X-Ray Scattering (WAXS) experiments were performed  
186 using a Rigaku DMAX-II diffractometer. Diffraction patterns were obtained in the range  $5^\circ < 2\theta < 60^\circ$  with Cu-  
187  $K\alpha$  radiation ( $\lambda = 1.5405 \text{ \AA}$ ) under the following conditions: 40 kV, 40 mA, step width 0.02°, time per step 2  
188 sec, divergence slit 0.25°, Soller slit 0.04 rad and antiscatter slit 0.5°. X-Ray patterns are normalized on the  
189 main peak.  
190  
191 **Films Casting.** Films for WAXS analyses were obtained from a chloroform solution; 10 grams of polymer were  
192 dissolved into 50 grams of  $\text{CHCl}_3$ . The solution was cast on a glass surface and the solvent was evaporated at  
193 room temperature and pressure overnight. Film thickness was determined by Nikon eclipse ME600 optical  
194 microscope with Nikon digital camera light DS-Fil, software NIS-Element BR, and magnification 50x, and it  
195 was in the range 60-90  $\mu\text{m}$ .  
196  
197 **Transmission Electron Microscopy (TEM) analysis.** For the analysis of CNC, drops of aqueous dispersions of  
198 CNC (1 wt%) were deposited on carbon-coated electron microscope grids, negatively stained with uranyl  
199 acetate and allowed to dry. For the analysis of nanocomposites, a representative sample was chosen: PLA5  
200 was cut with a microtome and the slices obtained were negatively stained with uranyl acetate. Samples were  
201 analyzed with a Hitachi Jeol-10084 TEM operated at an accelerating voltage of 80 kV.  
202  
203 **Fourier Transform Infrared Spectroscopy (FT-IR).** FT-IR Spectrometer (Spectrum 100, PerkinElmer) with an  
204 attenuated total reflection (ATR) was used to register spectra for PLA sample, all nanocomposites and CNC  
205 alone. FT-IR spectra of PLA, CNC and PLA5 are shown in the Supporting Information file. Significant peaks for  
206 PLA/Nanocomposites: 1747  $\text{cm}^{-1}$  (C=O stretching), 1000-1200 $\text{cm}^{-1}$  (C-O stretching). Significant peaks for CNC:  
207 3335  $\text{cm}^{-1}$  (-OH stretching), 1032  $\text{cm}^{-1}$  (C-O stretching).  
208  
209  **$^1\text{H}$  NMR analyses.**  $^1\text{H}$  NMR spectra for PLA sample and nanocomposites were registered with a Bruker  
210 Ultrashield 400 MHz. The chemical shifts are reported in ppm and referred to TMS as internal standard. All  
211 samples were prepared by dissolving 6-8 mg of polymer into 1 mL of  $\text{CDCl}_3$ . Spectra of PLA and PLA5 are

212 shown in the Supporting Information file. Peaks attribution for the  $^1\text{H}$  NMR (400 MHz,  $\text{CDCl}_3$ ):  $\delta$  5.18 (H-1, q,  
213  $J = 4$  Hz), 1.60 (H-2, d,  $J = 4$  Hz).

214

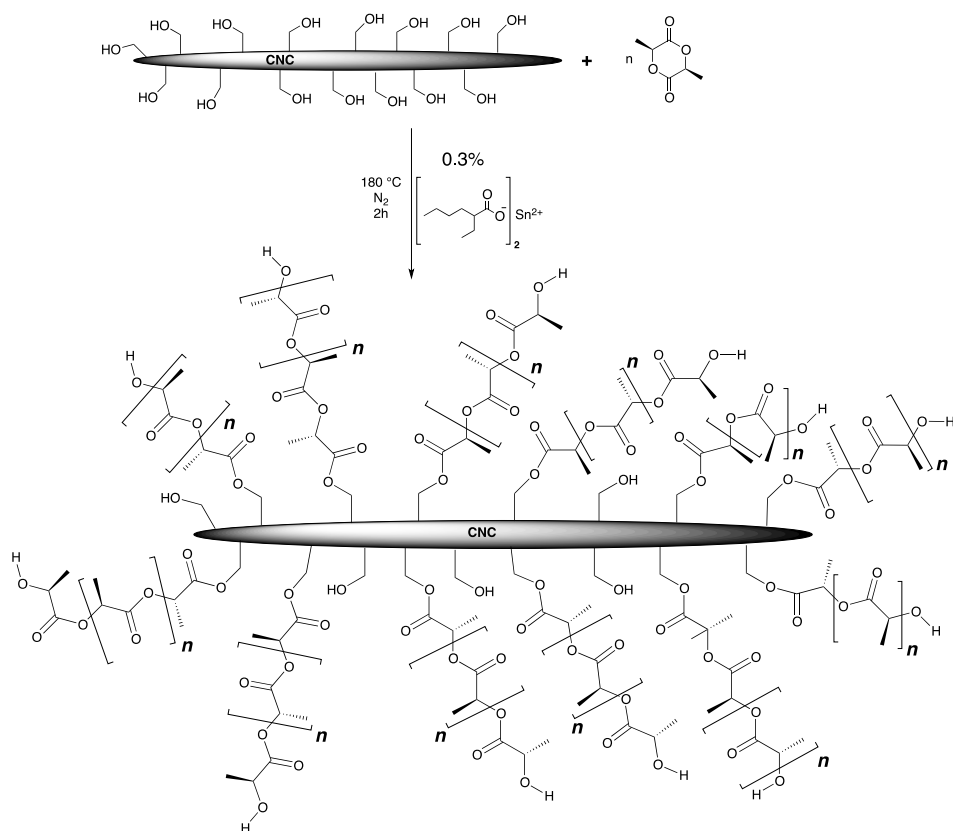
## 215 Results and discussion

216

### 217 Synthesis of PLA-CNC nanocomposites.

218 A schematic representation of the *in situ* synthesis of PLA-CNC nanocomposites is reported in **Scheme 1**. The  
219 product of the reaction is likely to be a complex mixture of species, with both free PLA chains and PLA-grafted  
220 CNC. Free PLA shows a molecular weight distribution from SEC analyses. CNC can be characterized by  
221 different degrees of functionalization.

222



223

224 **Scheme 1:** schematic representation of the *in situ* synthesis of PLA-CNC.

225 Synthesis provided semi-crystalline materials characterized by an increasing brownish shade as the  
226 concentration of nanocrystals increased. The polymers are homogeneous and no CNC are visible, indicating  
227 an optimal dispersion within the nanocomposite.

228

### 229 Size exclusion chromatography (SEC)

230 SEC curves were obtained for all samples. As described in experimental section, samples were filtered on  
231  $0.45 \mu\text{m}$  filters before the analysis, therefore SEC data refer only to the polymer present in solution.

232 In **Figure 1** selected SEC graphs (PLA, PLA0.5 and PLA3) are reported. Curves have been normalized with  
233 respect to the peak relative to the most abundant polymeric species for all samples. As expected, PLA SEC

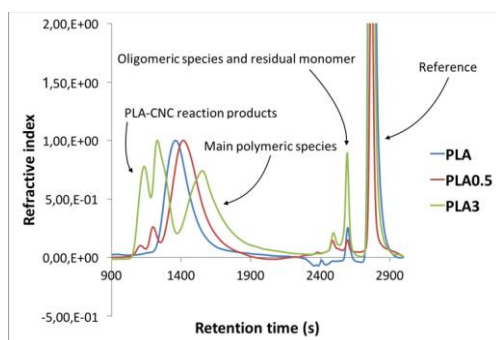
234 curve shows only a peak at low retention time, related to the polymer. The peaks between 2400 secs and  
 235 2700 secs are attributable to low molecular weight species and residual monomer. PLA0.5 and PLA3 samples,  
 236 containing 0.5 wt.% and 3 wt.% of CNC respectively, show two additional peaks at very low retention times  
 237 (around 1100 secs and 1200 secs). It should be noted that such peaks get more intense as the wt.% of CNC  
 238 increases. Given the presence of additional peaks,  $\overline{M}_n$  and  $\overline{M}_w$  values for CNC-containing nanocomposites  
 239 cannot be considered reliable. For this reason, only  $M_p$  values are presented in **Table 2**, where  $M_p$  refers to  
 240 the peak around 1400-1700 secs.  $M_p$  can be defined as the mass value for the most abundant species in  
 241 chromatogram. Observing the trend moving from PLA to PLA0.5 and PLA3 graphs, it can be stated that the  
 242 peak around 1400-1700 secs is attributable to "standard" PLA chains, straightly obtained through ROP of  
 243 lactide. Hydroxyl groups present as moisture in the polymerization apparatus and the small quantity of lactic  
 244 acid present together with lactide likely promote such conventional process.  
 245 However, employing CNC in the *in situ* polymerization process, covalently bound CNC are also obtained, as  
 246 CNC can act as initiators through their hydroxyl groups, affording various possible CNC containing polymeric  
 247 species.  
 248 From **Figure 1**, it could be noted that higher wt.% of CNC present in the feed leads to a decrease of molecular  
 249 weight of standard PLA chains. This datum strongly supports the hypothesis that free OH groups on CNC's  
 250 surface participate in the ROP of lactide. In fact, as the CNC's concentration increases in the feed, more  
 251 initiators will be actually present, leading to shorter chains. The additional peaks which are present in the  
 252 SEC-graphs of PLA0.5 and PLA3 at very high hydrodynamic volumes are likely attributable to polymeric  
 253 species containing covalently bound CNC. In order to exclude the possibility that such peaks are due to CNC  
 254 themselves, SEC analysis of CNC alone was also performed in the same experimental conditions. No signals  
 255 were registered, confirming that such peaks in the chromatograms of PLA-CNC can only be related to  
 256 nanocomposites produced by chemical reaction of CNC with lactide. In principle, further macromolecular  
 257 entities could be also formed from CNC and lactide, whose dimensions are larger than those of filter pores  
 258 used for SEC.

259  
260  
261  
262  
263

SAMPLE	CNC CONTENT (%W/W)	$M_p$ (Da)
PLA	0	283600
PLA0.5	0.5	182400
PLA2	2	110600
PLA2.5	2.5	81900
PLA3	3	55000
PLA5	5	53500

**Table 2:** Peak molecular weight for synthesized nanocomposites relative to peaks between 1400 and 1700 sec.

264



265  
266  
267 **Figure 1:** SEC graphs for PLA, PLA0.5 and PLA3 samples.  
268

### 269 **Thermal analyses (DSC)**

270 **Figure 2** reports the second heating scan for DSC thermograms of all samples, compared to the thermogram  
271 of standard PLA. All samples show similar behavior. Indeed, after the first heating cycle necessary to eliminate  
272 residual internal stresses deriving from the synthesis, they do not crystallize during cooling. Crystallization  
273 occurs during the second heating (cold crystallization), affording a crystalline phase which is characterized by  
274 two melting peaks. It can be noted that the peak at lower temperature becomes more intense as the wt.%  
275 of CNC increases. It is well known<sup>28, 29</sup> that PLA can crystallize in three different forms, depending on the  
276 crystallization conditions, namely  $\alpha$ ,  $\beta$  and  $\gamma$  forms. Crystallization from the melt above 120 °C results in the  
277 formation of stable crystals labeled as  $\alpha$ -crystals. They are characterized by the packing of two chain  
278 segments with a 10<sub>3</sub> helical conformation to form an orthorhombic unit cell. The  $\alpha$ -form is the most common  
279 PLA crystalline phase, while  $\beta$  and  $\gamma$  ones form through different thermal/mechanical treatments.

280 It has been demonstrated<sup>30, 31</sup> that, when crystallization from the melt occurs with isothermal analyses at  
281 temperatures lower than 120 °C, the formation of more disordered and metastable  $\alpha'$ -crystals is promoted.  
282 Such crystals show slightly larger unit-cell dimensions as well as lower packing density in comparison to  $\alpha$ -  
283 crystals. Their existence can explain the splitting of melting peaks in PLA, observed also in previous  
284 literature.<sup>32</sup>

285 Coming to our DSC experiment, the high regularity of the chains in the standard PLA sample leads to the  
286 formation of  $\alpha$ -crystals during cold crystallization, resulting in a single melting peak, bearing a slight shoulder  
287 at lower temperature, probably due to a small presence of  $\alpha'$ -crystals. When CNC are added in the  
288 polymerization feed, giving rise to *in situ* polymerization with lactide, they probably lead to more disordered  
289 crystals, with the melting peak at lower temperature becoming more and more evident as CNC wt.%  
290 increases. This seems to indicate that the higher is the wt.% of CNC, the more favored will be the formation  
291 of  $\alpha'$ -phase. From **Figure 2** it can also be noticed that cold crystallization temperature increases as the wt.%  
292 of CNC increases.

293 Analyzing DSC data, reported in **Table 3**, it appears that CNC make crystallization of PLA more difficult.  
294 Interestingly, in literature data relative to PLA-CNC blends, an opposite trend is reported, i.e. an improvement  
295 in crystallization kinetics with respect to standard PLA.<sup>33</sup> In those cases, nanocrystals seem to have a  
296 nucleating effect, favoring the formation of crystals. It appears, however, that an increase in affinity between  
297 PLA and CNC (i.e. by modification through grafting approaches) leads to lower crystallization kinetics.<sup>20, 24</sup> In  
298 particular, it was hypothesized that the greater is the adhesion of polymer chains onto nanocrystals surface,  
299 the lower is the mobility for chains themselves, with consequent slowing in crystals' formation.

300 In our nanocomposites, CNCs act presumably as disturbing agents for crystallization since the chemical  
301 anchoring onto nanocrystals surface brings to a decrease of the degrees of freedom for polymeric chains.  
302 This eventually leads to a more difficult organization of macromolecules and, therefore, to a more difficult  
303 formation of crystals.  
304

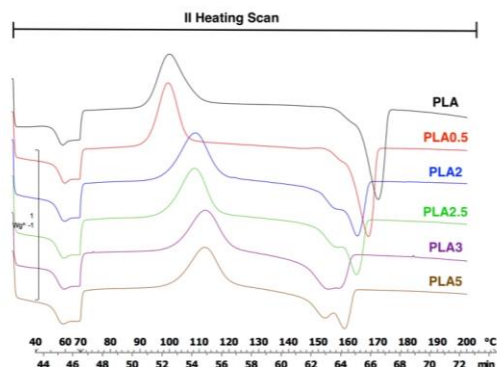


Figure 2: DSC thermograms for all samples.

Sample	$T_g$ (°C)	$T_{cc}$ (°C)	$T_m$ (°C)
PLA	54	100	170
PLA0.5	53	99	166
PLA2	54	109	163
PLA2.5	54	108	163
PLA3	54	112	157
PLA5	53	112	159

Table 3: thermal DSC data for all samples

### Thermal analyses (TGA)

Figure 3 shows TGA curves of all PLA-CNC nanocomposites. All samples show a single step degradation pathway. Thermal stabilities of PLA nanocomposites were evaluated from TGA thermograms checking temperatures corresponding to 5%, 30%, 50% and 95% of weight loss ( $T_{5\%}$ ,  $T_{30\%}$ ,  $T_{50\%}$  and  $T_{95\%}$  respectively). It has to be pointed out that all nanocomposites show higher thermal stability in comparison to standard PLA. This result marks an important difference from what reported for PLA-CNC nanocomposites obtained via compounding, for which a decrease, or in the best cases no variations in thermal stability in comparison to PLA are detected.<sup>18, 19</sup> It must be considered that CNC are routinely obtained through  $H_2SO_4$ -based hydrolysis of cellulose fibers and they are therefore recovered bearing sulfate groups. It is reported that thermal stability of CNC is strongly related to the acidity of the sulfate groups on the crystals surface,<sup>17, 34, 35</sup> i.e. the higher is the quantity of sulfate groups, the easier is expected to be the thermal degradation. Most likely, this is the reason also for the observed enhanced thermal degradation in the case of physical mixtures between PLA and CNC.

Functionalization of CNC with different moieties has been explored, in order to obtain a higher thermal stability of crystals themselves and, in turn, of resulting nanocomposites.<sup>20</sup> In almost all reported cases, however, no improvements were registered for what regards the thermal stability of the materials obtained. An increase of thermal degradation temperature (around 12 °C in the best case) was reported by Dhar and co-workers, when the reactive extrusion process was adopted (see Introduction).<sup>25</sup> In this latter case  $T_{onset}$  increased of about 12 °C and  $T_{50\%}$  of around 5 °C.

As shown by the data reported in Table 4, all PLA-CNC samples show higher degradation temperatures with respect to standard PLA. Among reported data,  $T_{5\%}$ , corresponding to 5% weight loss, can be considered as the starting point for thermal degradation. It appears that all nanocomposites show improved thermal resistance, with  $T_{5\%}$  that increases up to 25 °C in the best case in comparison to standard PLA. The difference in weight loss between standard PLA and nanocomposites becomes less pronounced with the increase of

344 temperature. It has to be said, however, that all CNC containing samples appear to possess higher  $T_{30\%}$  (up  
345 to  $\sim 25$  °C) and higher  $T_{50\%}$  (up to  $\sim 14$  °C), indicating a marked improvement over best previous literature  
346 results.

347 The improvement of thermal stability for nanocomposites can be hypothetically ascribed to two factors.  
348 From one side it is reasonable to think that reaction between CNC and L-lactide allows to “mask” the  
349 deleterious sulfate groups that otherwise would increase thermal degradation.

350 Secondly, it is possible that, the reduced mobility of chains due to their linkage to nanocrystals allows a better  
351 thermal stability, making chains stiffer and less prone to oxidation and degradation reactions.

352

353

354

355

356

357

358

359

360

361

362

SAMPLE	$T_{5\%}$ (°C)	$T_{30\%}$ (°C)	$T_{50\%}$ (°C)	$T_{95\%}$ (°C)
PLA	262	301	325	360
PLA0.5	279	314	330	353
PLA2	281	325	340	361
PLA2.5	286	322	335	359
PLA3	282	320	332	358
PLA5	286	322	335	366

Table 4: Thermal degradation temperatures corresponding to defined weight losses for all samples.

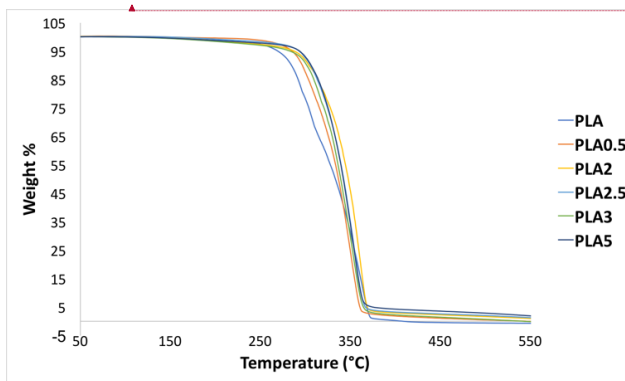


Figure 3: TGA curves for all samples.

Formattato: Posizione: Orizzontale: 7,11 cm, Rispetto a: Pg, Verticale: 5,09 cm, Rispetto a: Paragrafo

Formattato: Tipo di carattere: Corsivo, Colore carattere: Automatico

Formattato: Normale, Allineato a sinistra, Posizione: Orizzontale: 7,11 cm, Rispetto a: Pg, Verticale: 5,09 cm, Rispetto a: Paragrafo

363

364

365

366

367

368

Rheological analyses

369 Since the reinforcing effect of CNC in PLA matrices is well known,<sup>36, 37</sup> we performed rheological analyses, in  
 370 order to evaluate the effect of the *in situ* polymerization protocol on the complex viscosity and storage  
 371 modulus. As the wt.% of CNC increases, two effects can be observed. From one side, the high rigidity of CNC  
 372 contributes to increase the melt viscosity. This trend is in contrast with the related decrease in molecular  
 373 weight of the PLA polymer, observed by SEC, that acts in the opposite direction, lowering the melt viscosity.  
 374 Rheological curves obtained via frequency sweep experiments are reported in **Figure 4** for all samples.  
 375 Sample PLA0.5 shows viscoelastic behavior with a Newtonian plateau at low shear rates and a shear thinning  
 376 behavior. PLA sample shows a decrease in viscosity at low shear rates, caused by partial degradation of the  
 377 sample during the analysis: in PLA0.5 such effect is not visible, probably thanks to the thermal stabilizing  
 378 effect of CNC, as explained in TGA paragraph. Although all materials behave as thermoplastics, with the  
 379 increase of wt.% CNC samples tends to have an increased shear sensitivity in all range of frequencies. This  
 380 behavior is marked for PLA 2 and PLA3 samples.  
 381 Storage ( $G'$ ) modulus curves (**Figure 5**) show that PLA sample has the typical behavior of a thermoplastic  
 382 polymer, with the low shear zone slope of  $G'$  curve being around 2. With the increase of CNC wt.%, the slope  
 383 of the curve becomes significantly lower and the whole  $G'$  plot tends to a straight line. A trend of this type  
 384 can be attributed to the progressive transition from liquid- to solid-like behavior, which therefore indicates  
 385 a good dispersion of nanoparticles into the polymeric matrix. As expected, PLA0.5 shows the smallest  
 386 difference with standard PLA.  
 387

388  
389

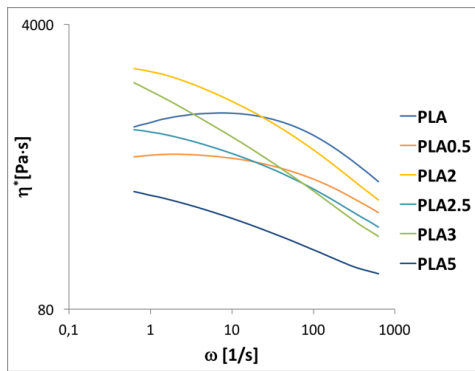


Figure 4: complex viscosity curves for all samples.

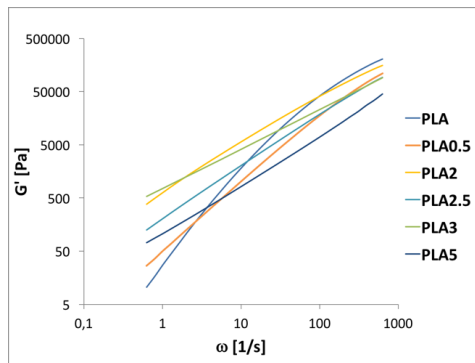


Figure 5: storage modulus curves for all samples.

390  
391

392

Sample	$G'$ [Pa]	
	at $\omega = 628.3 \text{ s}^{-1}$	at $\omega = 0.6823 \text{ s}^{-1}$
PLA		
PLA0.5		
PLA2		
PLA2.5		
PLA3		
PLA5		

PLA	205800	10
PLA0.5	110300	26
PLA2	154600	381
PLA2.5	92950	126
PLA3	90490	537
PLA5	45380	72

**Table 5:** storage modulus values at the two extremes of the curves.

393

394

395 In **Table 5** storage modulus values at  $\omega = 628.3 \text{ s}^{-1}$  and at  $\omega = 0.6823 \text{ s}^{-1}$ , which are the extremes of the curves,  
 396 are reported. The trend just described is here well highlighted, with PLA sample that shows the highest  $G'$  at  
 397 high frequency and the lowest at low frequency, while all nanocomposites show a less pronounced decrease  
 398 of storage modulus values.

399

400

#### WAXS Analyses

401 Crystalline structure of PLA and PLA-CNC nanocomposites was studied through WAXS analyses on films  
 402 obtained by casting from a PLA solution in  $\text{CHCl}_3$  as previously described. As **Figure 6** shows, PLA sample  
 403 appears to have four characteristic peaks at  $2\theta = 14.60^\circ$ ,  $16.68^\circ$ ,  $19.14^\circ$  and  $22.27^\circ$ , as already reported in  
 404 literature.<sup>38</sup> Crystallinity of PLA0.5 sample seems to be not significantly affected by the presence of cellulose  
 405 nanocrystals. As concentration of CNC increases, however, the crystallinity of nanocomposites decreases. In  
 406 the case of PLA2 signals relative to PLA are still present. However they are less sharp and the peak at  $22.27^\circ$   
 407 is barely appreciable. An additional increase of concentration (namely PLA2.5, PLA3 and PLA5 samples) brings  
 408 to a further decreased of crystallinity. These three nanocomposites show a broad peak centered around  $2\theta$   
 409  $= 16^\circ$  and characteristic PLA peaks are not detectable anymore. Interestingly, however, it should be noted  
 410 that with the increase in w/w% of CNC, the crystalline peak of PLA shifts towards lower values of  $2\theta$ . To this  
 411 regard, it is well known in literature that the peak at  $2\theta = 16.7^\circ$  is relative to  $\alpha$  crystalline phase of PLA.<sup>16</sup> This  
 412 signal shifts as the contribution of  $\alpha'$  form becomes higher, reaching values equal to  $2\theta = 16.4^\circ$ .<sup>39,40</sup> As **Figure**  
 413 **6** shows, all nanocomposites with except of PLA0.5, show lower values of  $2\theta$  in this spectral region, therefore  
 414 confirming DSC data regarding the presence of differently ordered crystalline phases.

415 In addition, it appears that for samples with the highest concentrations of CNC, the signals pattern of  
 416 nanocrystals becomes more and more evident. As shown in **Figure 7**, CNC show four main peaks at  $2\theta =$   
 417  $14.79^\circ$ ,  $16.58^\circ$ ,  $22.83^\circ$  and  $45.23^\circ$ . The peak at  $2\theta = 32^\circ$  is spurious and presumably related to  $\text{K}_2\text{SO}_4$  generated  
 418 during the extraction of nanocrystals. Meanwhile the two peaks at  $14.79^\circ$  and  $16.58^\circ$  respectively cannot be  
 419 detected under the broad signal in PLA2.5, PLA3 and PLA5 samples. It appears that the other two peaks  
 420 appear with increasing intensity as the concentration of CNC increases in the material. In particular, for what  
 421 regards PLA5, both a shoulder around  $22.5^\circ$  and a peak around  $54.5^\circ$  are present, closely resembling signals  
 422 relative to pure CNC. It is therefore reasonable to think that at high concentration of CNC the dispersion of  
 423 nanocrystals in the matrix becomes less efficient, leading to the presence of some CNC crystalline domains.

424

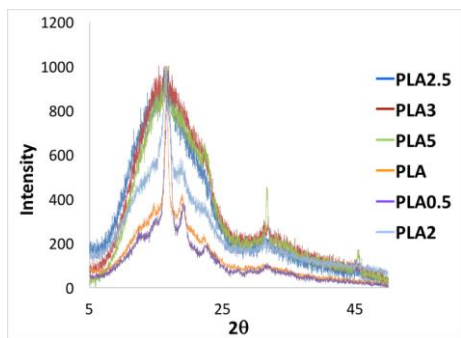


Figure 6: WAXS diffractograms for all nanocomposites and PLA sample.

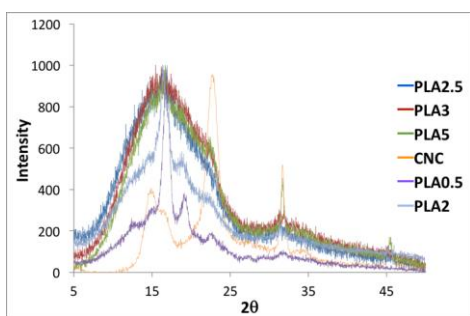


Figure 7: WAXS diffractograms for all nanocomposites and CNC sample.

### TEM analyses

The dimensions of cellulose nanocrystals used for the preparation of nanocomposites were determined via TEM. In Figure 8 a TEM image of CNC is reported.

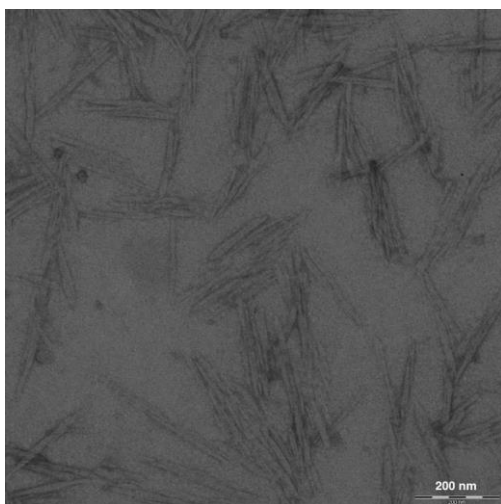
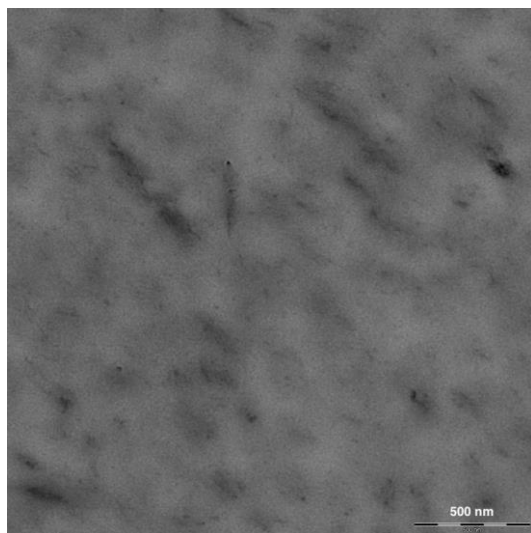


Figure 8: TEM micrograph of CNC.

437 Cellulose nanocrystals have an average length of  $195 \pm 28$  nm and an average diameter of  $16 \pm 4$  nm, resulting  
438 in an aspect ratio of  $13 \pm 4$ .  
439 In **Figure 9** a TEM micrograph of PLA5 is reported. PLA5 was chosen because it is the sample having the higher  
440 content of CNC among all nanocomposites samples. In **Figure 9**, CNC can be distinguished over the polymeric  
441 matrix as randomly distributed dark halos.  
442



443  
444 **Figure 9:** TEM micrograph of PLA5 sample.

445 CNC are not clearly different from the polymeric matrix, differently from what reported for CNC-PLA blends.<sup>41</sup>  
446 Such difference can be ascribed to the scarce affinity between CNC and PLA in classical blends, which results  
447 in a distinct separation of the two phases. In our case, the *in situ* growth of PLA chains onto CNC surface  
448 allows the crystals to be fully embedded in the polymer, with an intimate interfacial contact.  
449 It is also important to note that crystals' dimensions in PLA5 appear to be of the same order of magnitude as  
450 in CNC alone, even if dimensions cannot be accurately determined because of the indefinite profile of  
451 dispersed crystals. Again, this result underlines a clear morphological difference between nanocomposites  
452 here described and PLA-CNC blends, in which the formation of CNC agglomerates is reported.<sup>42</sup> The uniform  
453 dispersion within the polymeric matrix is another proof of the efficacy of the *in situ* approach for the  
454 preparation of PLA-CNC nanocomposites even at relatively high loadings of CNC.

#### 455 **FT-IR and <sup>1</sup>H NMR analyses**

457 In PLA FT-IR spectrum the peak relative to ester carbonyl groups can be recognized at  $1747\text{ cm}^{-1}$ , as well as  
458 signals between  $1000$  and  $1200\text{ cm}^{-1}$  can be ascribed to C-O bonds in aliphatic esters. CNC spectrum is  
459 characterized by the presence of a strong signal at  $3335\text{ cm}^{-1}$  that can be attributed to the free OH groups on  
460 crystals surface. The intense band at  $1032\text{ cm}^{-1}$  can be attributed to C-O ether bonds in cellulose.  
461 Nanocomposites spectra closely resemble the standard PLA spectrum although some typical CNC peaks are  
462 however visible. The hypothesis is that PLA chains fully cover the CNC surface, preventing most of typical  
463 cellulose signals to be detected.

464 <sup>1</sup>H NMR analyses show no significant differences between the spectra of PLA and nanocomposites, with the  
465 presence of a quartet signal centered at 5.18 ppm, relative to hydrogen in  $\alpha$  position with respect to the  
466 carbonyl group and a doublet signal centered at 1.60 ppm relative to the methyl group.

467  
468  
469 **Conclusions**

470 In this work, cellulose nanocrystals were successfully synthesized, starting from cotton linters through acidic  
471 hydrolysis, and they were subsequently used for *in situ* melt polymerization of PLA.  
472 Full characterization of nanocomposites has been performed, aimed to investigate the effect of CNC on the  
473 morphological and thermo-mechanical properties of materials.  
474 Through SEC analysis it has been possible to assess the actual occurrence of chemical bonds between CNC  
475 and PLA chains. Indeed, as the quantity of added CNC increases, the molecular weight of the polymer  
476 decreases, possibly indicating a role of free OH groups on cellulose surface, as initiators during the *in situ*  
477 polymerization process.  
478 DSC analyses were performed to evaluate the thermal behavior of the materials. The presence of CNC in the  
479 reaction system seems to favor the formation of  $\alpha'$  crystals, which are less ordered with respect to the more  
480 common  $\alpha$  crystal form in PLA. Again, it can be argued that free OH groups act as initiators, perhaps forming  
481 complex star-like macromolecular architectures which are more prone to form less ordered crystals.  
482 From TGA analyses it has been clearly demonstrated that synthesized bionanocomposites show a marked  
483 improvement in thermal stability with respect to standard PLA. Results indicate an improvement also with  
484 respect to literature data regarding the thermal stability of various types of PLA-CNC nanocomposites.  
485 Finally, nanocomposites show an improvement in rheological properties with respect to standard PLA. In  
486 particular it has been shown that storage modulus markedly increases in the presence of CNC, indicating a  
487 reinforcing effect given by these species.  
488 In conclusion, the described *in situ* synthetic methodology allows not only an optimal compatibilization  
489 between the two entities, facing one of the major problems inherent to the preparation of nanocomposites,  
490 but also leads to remarkably improved thermal and rheological properties of the obtained materials, with  
491 respect to standard PLA and conventional PLA-CNC nanocomposites. Among tested CNC concentrations, the  
492 2 %w/w appeared to be the most promising. In fact, while TGA data remain very similar for all  
493 nanocomposites, PLA2 sample proved to possess the best rheological properties, probably thanks to a  
494 combination of high molecular weight and reinforcing effect given by CNC.  
495

## 496 Notes and references

- 497 1 Inkinen, S.; Hakkarainen, M.; Albertsson, A.; Sodegard, A.; *Biomacromolecules*; 2011; **12**; 523-532.
- 498 2 Datta, R.; Henry, M.; *J. Chem. Technol. Biotechnol.*; 2006; **81**; 1119-1129.
- 499 3 Armentano, I.; Bitinis, N.; Fortunati, E.; Mattioli, S.; Rescignano, N.; Verdejo, R.; Lopez-Manchado, M.A.; Kenny, J.M.;  
500 *Progress in Polymer Science*; 2013; **38**; 1720-1747.
- 501 4 Lunt, J.; *Polymer Degradation and Stability*; 1998; **59**; 145-152.
- 502 5 Auras, R.; Harte, B.; Selke, S.; *Macromol. Biosci.*; 2004; 835-864.
- 503 6 Raquez, J.M.; Habibi, Y.; Murariu, M.; Dubois, P.; *Progress in Polymer Science*; 2013; **38**; 1504-1542.
- 504 7 Ramontja, J.; Sinha Ray, S.; Pillai, S.K.; Luyt, A.S.; *Macromol. Mater. Eng.*; 2009; **294**; 839-846.
- 505 8 Kaseem, M.; Hamad, K.; Deri, F.; Gun Ko, Y.; *Polym. Bull.*; 2016.
- 506 9 Sabatini, V.; Farina, H.; Basilissi, L.; Di Silvestro, G.; Ortenzi, M.A.; *Journal of Nanomaterials*; 2015; 1-16.
- 507 10 Castiello, S.; Coltelli, M.B.; Conzatti, L.; Bronco, S.; *Journal of Applied Polymer Science*; 2012; **125**; E413-E428.
- 508 11 Basilissi, L.; Di Silvestro, G.; Farina, H.; Ortenzi, M.A.; *J. App. Polym. Sci.*; 2013; 1575-1582.
- 509 12 Ortenzi, M.A.; Basilissi, L.; Farina, H.; Di Silvestro, G.; Piergiorganni, L.; Mascheroni, E.; *European Polymer Journal*; 2015; **66**;  
510 478-491.
- 511 13 Ioelovich, M.; *BioResources*; 2008; **3**; 1403-1418.
- 512 14 Trache, D.; Hazwan Hussin, M.; Mohamad Haafiz, M. K.; Kumar Thakur, V.; *Nanoscale*; 2017.
- 513 15 Mascheroni, E.; Rampazzo, R.; Ortenzi, M. A.; Piva, G.; Bonetti, S.; Piergiorganni, L.; *Cellulose*; 2016; **23**; 779-793.
- 514 16 Dhar, P.; Tarafder, D.; Kumar, A.; Katiyar, V.; *RSC Adv.*; 2015; **5**; 60426-60440.
- 515 17 Ambrosio-Martin, J.; Fabra, M. J.; Lopez-Rubio, A.; Lagaron, J. M.; *Cellulose*; 2015; **22**; 1201-1226.
- 516 18 Pracella, M.; Minhaz-Ul Haque, Md.; Puglia, D.; *Polymer*; 2014; **55**; 3720-3728.
- 517 19 Spinella, S.; Lo Re, G.; Liu, B.; Dorgan, J.; Habibi, Y.; Leclere, P.; Raquez, J. M.; Dubois, P.; Gross, R. A.; *Polymer*; 2015; **65**; 9
- 518 20 Bledzki, A. K.; Gassan, J.; *Prog. Polym. Sci.*; 1999; **24**; 221-274.
- 519 21 Lizundia, E.; Fortunati, E.; Dominici, F.; Vilas, J. L.; Leon, L. M.; Armentano, I.; Torre, L.; Kenny, J. M.; *Carbohydrate*  
520 *Polymers*; 2016; **142**; 105-113.
- 521 22 Mujica-Garcia, A.; Hooshmand, S.; Skrifvars, M.; Kenny, J. M.; Oksman, K.; Peponi, L.; *RCS Adv.*; 2016; **6**; 9221-9231.
- 522 23 Goffin, A. L.; Raquez, J. M.; Duquesne, E.; Siqueira, G.; Habibi, Y.; Dufresne, A.; Dubois, P.; *Biomacromolecules*; 2011; **12**;  
523 2456-2465.
- 524 24 Dhar, P.; Tarafder, D.; Kumar, A.; Katiyar, V.; *Polymer*; 2016; **87**; 268-282.
- 525 25 Yang, W.; Dominici, F.; Fortunati, E.; Kenny, J.M.; Puglia, D.; *RSC Adv.*; 2015; **5**; 32350-32357.

- 526 26 Nakayama, N.; Hayashi, T.; *Polymer degradation and stability*; 2007; **92**; 1255-1264.
- 527 27 Kaewprapan, K.; Phattananudee, S.; *J. Nanosci. Nanotechnol.*; 2012; **12**; 781-786.
- 528 28 Kawai, T.; Rahman, N.; Matsuba, G.; Nishida, K.; Kanaya, T.; Nakano, M.; Okamoto, H.; Kawada, J.; Usuki, A.; Honma, N.;  
529 Nakajima, K.; Matsuda, M.; *Macromolecules*; 2007; **40**; 9463-9469.
- 530 29 Cocca, M.; Di Lorenzo, M. L.; Malinconico, M.; Frezza, V.; *European Polymer Journal*; 2011; **47**; 1073-1080.
- 531 30 Righetti, M. C.; Gazzano, M.; Di Lorenzo, M. L.; Androsch, R.; *European Polymer Journal*; 2015; **70**; 215-220.
- 532 31 Zhang, J.; Tashiro, K.; Tsuji, H.; Domb, A. J.; *Macromolecules*; 2008; **41**; 1352-1357.
- 533 32 Di Lorenzo, M. L.; Androsch, R.; *Macromol. Chem. Phys.*; 2016.
- 534 33 Gardebjer, S.; Bergstrand, A.; Idstrom, A.; Borstell, C.; Naana, S.; Nordstierna, L.; Larsson, A.; *Composites Science and  
535 Technology*; 2015; **107**; 1-9.
- 536 34 Lu, P.; Hsieh, Y. L.; *Carbohydrate Polymers*; 2010; **82**; 329-336.
- 537 35 Roman, M.; Winter, W. T.; *Biomacromolecules*; 2004; **5**; 1671-1677.
- 538 36 Bagheriasl, D.; Carreau, P. J.; Riedl, B.; Dubois, C.; Hamad, W. Y.; *Cellulose*; 2016; **23**; 1885-1897.
- 539 37 Kamal, M. R.; Khoshkava, V.; *Carbohydrate Polymers*; 2015; **123**; 105-114.
- 540 38 Ki, W. K.; Seong, I. W.; *Macromol. Chem. Phys.*; 2002; **203**; 2245.
- 541 39 Marubayashi, H.; Akaishi, S.; Akasaka, S.; Asai, S.; Sumita, M.; *Macromolecules*; 2008; **41**; 9192-9203.
- 542 40 Zhang, J.; Duan, Y.; Sato, H.; Tsuji, H.; Noda, I.; Yan, S.; Ozaki, Y.; *Macromolecules*; 2005; **38**; 8012-8021.
- 543 41 Sanchez-Garcia, M.D.; Lagaron, J.M.; *Cellulose*; 2010; **17**; 987-1004.
- 544 42 Gupta, A.; Simmons, W.; Schueneman, G.T.; Hylton, D.; Mintz, E.A.; *ACS Sustainable Chem. Eng.*; 2017; **5**; 1711-1720.